ARTICLE

Solution Chemistry of Self-Assembled Graphene Nanohybrids for High-Performance Flexible Biosensors

Bong Gill Choi,[†] HoSeok Park,[‡,*] Tae Jung Park,[§] Min Ho Yang,[†] Joon Sung Kim,[¶] Sung-Yeon Jang,[¶] Nam Su Heo,[§] Sang Yup Lee,[†,§] Jing Kong,[⊥] and Won Hi Hong[†,*]

[†]Department of Chemical & Biomolecular Engineering (BK21 program), KAIST, Daejeon 305-701, Korea, [‡]Department of Chemical Engineering, College of Engineering, Kyung Hee University, 1 Seochon-dong, Giheung-gu, Yongin-si, Gyeonggi-do 446-701, Korea, [§]BioProcess Engineering Research Center, Center for Systems & Synthetic Biotechnology, and Institute for the BioCentury, KAIST, Daejeon 305-701, Korea, [¶]Center for Energy Materials Research, Korea Institute of Science and Technology, P.O. Box 131 Cheongryang, Seoul 130-650, Korea, and [⊥]Department of Electrical Engineering and Computer Sciences, and Department of Physics, Massachusetts Institute of Technology, Cambridge, Massachusetts 02139

ABSTRACT We report the preparation of free-standing flexible conductive reduced graphene oxide/Nafion (RGON) hybrid films by a solution chemistry that utilizes self-assembly and directional convective-assembly. The hydrophobic backbone of Nafion provided well-defined integrated structures, on micro- and macroscales, for the construction of hybrid materials through self-assembly, while the hydrophilic sulfonate groups enabled highly stable dispersibility (~0.5 mg/mL) and long-term stability (2 months) for graphene. The geometrically interlocked morphology of RGON produced a high degree of mechanical integrity in the hybrid films, while the interpenetrating network constructed favorable conduction pathways for charge transport. Importantly, the synergistic electrochemical characteristics of RGON were attributed to high conductivity (1176 S/m), facilitated electron transfer (ET), and low interfacial resistance. Consequently, RGON films obtained the excellent figure of merit as electrochemical biosensing platforms for organophosphate (OP) detection, that is, a sensitivity of 10.7 nA/μM, detection limit of 1.37×10^{-7} M, and response time of <3 s. In addition, the reliability of RGON biosensors was confirmed by a fatigue test of 100 bending cycles. The strategy described here provides insight into the fabrication of graphene and hybrid nanomaterials from a material perspective, as well as the design of biosensor platforms for practical device applications.

KEYWORDS: graphene nanohybrid · self-assembly · functionalization · flexible electronics · biosensor

*Address correspondence to phs0727@khu.ac.kr, whhong@kaist.ac.kr.

Received for review January 25, 2010 and accepted April 2, 2010.

Published online April 8, 2010. 10.1021/nn100145x

Since the discovery of graphene by Geim *et al.* in 2004,[1] it has been touted as a "next generation material" because of its remarkable electronic, optical, and thermal properties, chemical and mechanical stability, and large surface area[1−10] for applications in both emerging and conventional fields such as field-effect transistors,[2] sensors,[3] electrochemical devices,[4,5] electromechanical resonators,[6] polymer nanocomposites,[7] batteries,[8] capacitors,[9] and light emitting devices.[10] Despite extensive research, a major challenge of graphene-based materials for practical applications is posed by the scalable dispersion and the long-term stability of sheet aggregates held together by van der Waals interactions.[11] Therefore, solution-based chemistry has been pursued to overcome these barriers.[12]

So far, several wet methods, so-called bench-marking techniques of processing carbon nanotubes (CNTs), have been shown to enhance the processability of graphene; control of pH, coating by small molecules, addition of surfactants or polymers, physical blending, and chemical functionalization.[11−19] In particular, the functionalization of polymers is a useful and powerful method for obtaining highly stable colloidal suspensions while simultaneously providing graphene with special properties.[12] Among a variety of functional polymers, Nafion, a perfluorosulfonated ionomer, can readily disperse graphene due to the intrinsic chemical structure consisting of a hydrophobic backbone and hydrophilic side chains. As a consequence of the role as an interfacial binder, Nafion efficiently assembles hybrid materials that are optimized for electrochemical applications. Compared to other polyelectrolytes, such as polystyrene sulfonate, Nafion showed better chemical and mechanical properties and higher electrical conductivity.[20,21] A gallery of nanohybrids, consisting of carbon-based materials and Nafion, performed better in comparison to other hybrids for application to electrochemical devices.[22] Furthermore, Nafion was able to effectively immobilize a variety of enzymes to facilitate biocatalytic electrochemical reactions for the detection of biomolecules.[22−24] Motivated by the lack of reports on the fabrication of reduced graphene oxide (RGO)/Nafion (RGON) hybrids and their

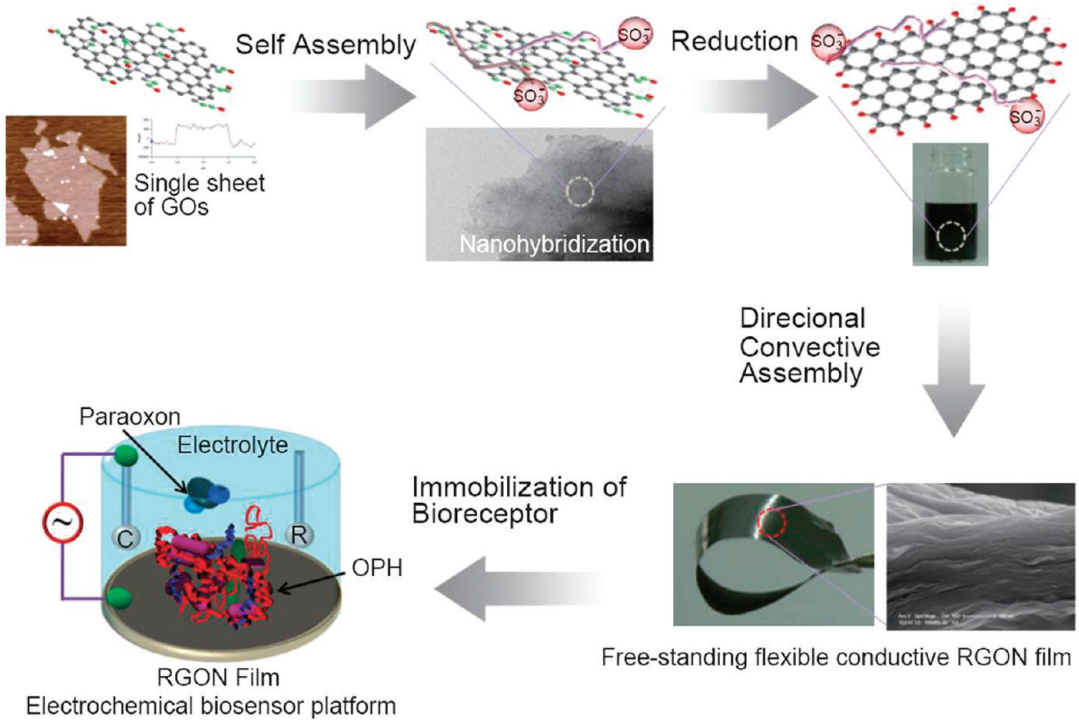

Scheme 1. Illustration of a procedure to design RGON hybrids and subsequently RGON platform for application in electrochemical biosensors.

electrochemical applications, we have investigated the solution-based preparation of highly stable conductive RGON hybrid films for application to electrochemical biosensors.

Graphene and its hybrid materials have been currently used, in the development of high performance electrochemical biosensors, as advanced electrodes because of their large accessible surface area, electrical conductivity, and capacity for immobilizing enzymes.[3,23,25] Niu *et al*. reported the application of graphene for an electrochemical glucose biosensor.[25] However, two polymers, polyethylenimine and polyvinylpyrrolidone, were used as the biosensor supporter, and the flexibility of the conductive film was not guaranteed. Lee *et al.* used Nafion as a binder to deposit nanometal-decorated graphene on an electrode.[3] However, they observed neither the dispersion of graphene by Nafion nor did they note that the hybrid films were self-standing. Instead, their films were deposited on a substrate. This limitation should be overcome by the development of new and simple techniques for preparing advanced sensing platforms for highly efficient electrochemical biosensors. In particular, the nanoscale hybridization of RGO with Nafion, delineated here, resulted in a synergistic effect for sensing performance due to a unique conduction mechanism that is different from those reported previously.

Our strategies for developing a free-standing flexible conductive biosensor platform are as follows: (1) graphene sheets were coated and functionalized through the self-assembly of the hydrophobic backbone of Nafion, (2) they were uniformly dispersed and stabilized by the high acidicity ($pK_a = -6$)[26] of sulfonic groups in the Nafion coating, (3) they were fabricated in the form of free-standing flexible robust films owing to the toughness of Nafion and the mechanical integrity of the hybrid, and (4) Nafion played a role in providing fast charge transport and low interfacial resistance for high performance of graphene-based biosensors. To demonstrate the merits of biosensor devices based on RGON hybrids, the resultant films were used for the detection of paraoxon substrate, which is an important biomolecule, and one of the most potent insecticides and chemical warfare agents. Remarkably, the as-prepared biosensors performed better as electrochemical sensors than other sensors described previously; specifically, they exhibited a sensitivity of 10.7 nA/μM, detection limitation of 1.37×10^{-7} M, response time of ~3 s, and ~90% of the maximum performance after 100 bending cycles.

RESULTS AND DISCUSSION

Solution Chemistry of Self-Assembled Graphene Nanohybrids. Scheme 1 illustrates the procedure for designing highly stable RGON hybrids and subsequently for fabricating the free-standing flexible conductive films of the resulting materials for application in biosensor devices. Starting from the commercial graphite and passing through the expanded graphite oxides, single layers of fully exfoliated GOs were prepared by the Hummers method.[27] The mixture of GO and Nafion was well dispersed in DI water/1-propanol bisolvent through sonication. The GOs were functionalized by the Nafion through partially hydrophobic interactions between the hydropho-

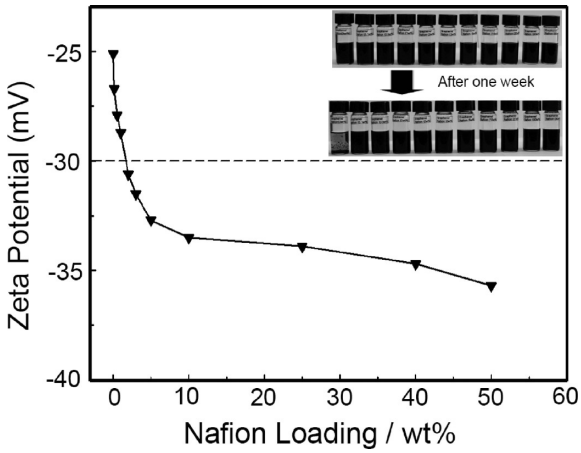

Figure 1. Zeta potentials of RGONs (0.5 mg/mL) on the Nafion loading levels in DI water/1-propanol (volume ratio of 50:50) bisolvent. Inset is the photographs of RGO and RGON solutions with respect to the contents of the Nafion from left: 0, 0.1, 0.5, 1, 2, 3, 5, 10, 25, 40, and 50 wt %.

bic backbone ($-CF_2-$) of the Nafion backbone and the hydrophobic part of basal planes in GOs as well as partially hydrophilic interactions between the sulfonic groups ($-SO_3H$) of the former and the polar groups such as hydroxyl, epoxy, and carboxylic acid groups of the latter. The coating of GOs by Nafion (GON) was proven by the TEM, FT-IR, and XPS results (see Figures S1, S2, and S3). A homogeneous colloid dispersion of RGON in bisolvent was obtained by the reduction of GO coated by Nafion polymer. The hydrophobic interactions between the Nafion backbone and RGO sheets were enhanced after the reduction step, by means of the restoration of the conjugated structures of RGO sheets and the conformational rearrangement of the amphiphilic Nafion in alcoholic solvent.[28,29] Most of the isolated GOs and RGONs were present as a single sheet by means of complete exfoliation, as verified by TEM, AFM, and XRD data (see Figures S4 and S5). The functionalization of RGO by Nafion was driven by self-assembly, which is attributed to the hydrophobic interactions between them. The free-standing flexible conductive RGON films were fabricated by the vacuum filtration (VF) method. VF is an effective and versatile method for preparing uniform carbon nanomaterial films through a directional convective flow-induced assembly, because the homogeneity of the films is guaranteed by the nature of the process itself.[30] To detect paraoxon, the organophosphorus hydrolase (OPH) enzymes were immobilized on the surface of RGON with preservation of biocatalytic activity. The detailed experimental procedures for preparing the platforms and OPH are provided in the Experimental Section.

The zeta potential was measured to explore the dispersion of RGO sheets in water/1-propanol bisolvent, triggered by functionalization with Nafion, as shown in Figure 1. The zeta potential values of RGONs decreased from −25.1 to −35.7 mV over the range of measurement. On the basis of dispersion (−33 mV) and conductivity (1176 S/m, 78% of RGO), 2 wt % Nafion was determined to be the optimum loading value for fabrication of the conducting hybrid films. In the nanocomposite system, low threshold values of physical properties were achieved by the homogeneous mixing of two phases.[31] Similarly, RGONs revealed dramatic changes in the zeta potential at low Nafion loadings due to the favorable interfacial characteristics and the high acidity of the sulfonic groups. Although RGONs obtained higher zeta potential values compared to −44.2 mV for pure Nafion under the same experimental conditions, Nafion contributed to the high dispersion of RGO (~0.5 mg/mL) and to the long-term stability observed over the course of 2 months. In the absence of Nafion, the dispersion of RGO was reduced, and aggregates were observed within 1 week. Given that the values of the zeta potential below −30 mV resulted in stable dispersion, from a general colloidal science perspective,[32] Nafion acts as a good dispersant in terms of providing a zeta potential of −30 mV even at the loading of 2 wt %.

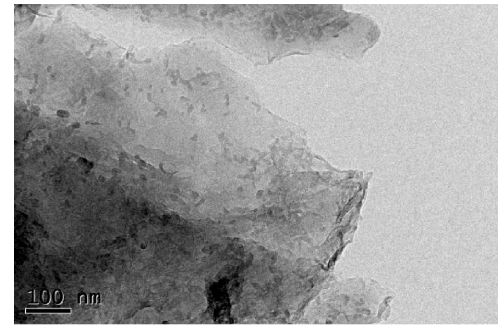

(A)

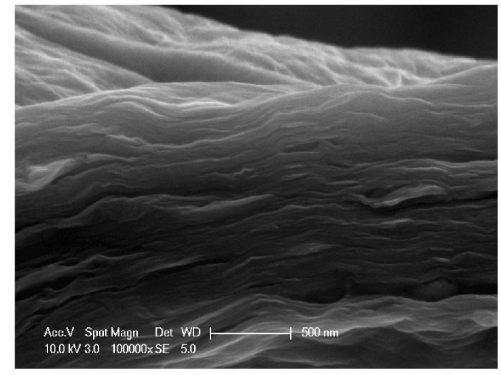

(B)

Figure 2. (A) TEM image of RGON hybrid and (B) SEM image of cross-section of RGON film.

Free-Standing Flexible Conductive Robust Graphene Nanohybrid Films. The micro- and macroscopic structures of hybrid films are another aspect of functionalization by Nafion that should be addressed. Figure 2A shows that individual RGO sheets were coated and dispersed by Nafion without aggregation, and a quality arises from the conformational changes of RGO and Nafion in bisolvent. It is worthwhile noting that the hydrophilic

groups ($-SO_3H$) of the Nafion enhanced the solubility of RGON in water, while the $-CF_2-$ groups of the Nafion backbone promoted the specific interactions with the RGO in alcoholic solvents. The interaction between Nafion and RGO was confirmed by FT-IR, XPS, XRD, NMR, and Raman spectroscopies (see Supporting Information, Figures S2, S3, S5, S6, and S7). Consequently, the functionalization by Nafion provided the colloidal dispersibility for RGO, while maintaining the conjugated structures. The self-assembly of RGON makes the edges of RGO sheets wrinkled in order to minimize the surface energy, similarly to the formation of nanoribbons by poly(*m*-phenylenevinylene-*co*-2,5-dioctoxy-*p*-phenylenevinylene).[2] Through favorable interactions and directional convective assembly, RGON was readily assembled into self-standing flexible robust hybrid films. The surface morphology of the RGON film was also observed by SEM (see Supporting Information, Figure S8). RGOs were compactly embedded in polymer matrices, stacked parallel to each other, and isolated completely by the entanglement of Nafion as shown in Figure 2B. In particular, the Young's modulus and tensile strength of RGON films displayed 46.3 GPa and 104.2 MPa which were much higher than those of flexible graphite foils as previously reported (see Supporting Information, Figure S9).[33] Analogous to the report of Shi *et al.*,[16] the interconnecting networks of the hybrid could be constructed by connections between Nafion-functionalized RGO layers during directional convective assembly. Therefore, geometric wrinkling of RGON induced mechanical integrity in the hybrid films due to the nanoscale sheet interlocking,[16] while the interpenetrating network of Nafion-coated RGOs formed favorable conduction pathways for charge transport.

Electrochemistry of Graphene Nanohybrid Films. Cyclic voltammetric analysis of redox reactions of $Fe(CN)_6^{3-}$/$Fe(CN)_6^{4-}$ is a typical method for evaluating the rate of electron transfer (ET) in carbon materials such as graphites, glassy carbons, and CNTs.[34,35] This system was chosen in order to investigate the intrinsic electrochemical behavior of RGON films. As shown in the typical cyclic voltammograms (CVs) of $Fe(CN)_6^{3-/4-}$ in Figure 3A, RGON films exhibited a sigmoidal shape with a peak-to-peak potential separation (ΔE_p) of 60 mV, which is related to the ET rate coefficient. A low ΔE_p for RGON films indicates a very fast ET rate that approaches ideal kinetics for a single-electron electrochemical reaction.[36] The Nernstian response is analyzed to verify the interfacial behavior of electroactive components in the process of adsorption and desorption.[37] In Nernstian or reversible systems, the peak current is obtained by the Randles–Sevčik method, described in eq 1,[37]

$$i_p = 0.4463\left(\frac{F^3}{RT}\right)^{1/2} n^{3/2} A D_o^{1/2} C_o \upsilon^{1/2} \qquad (1)$$

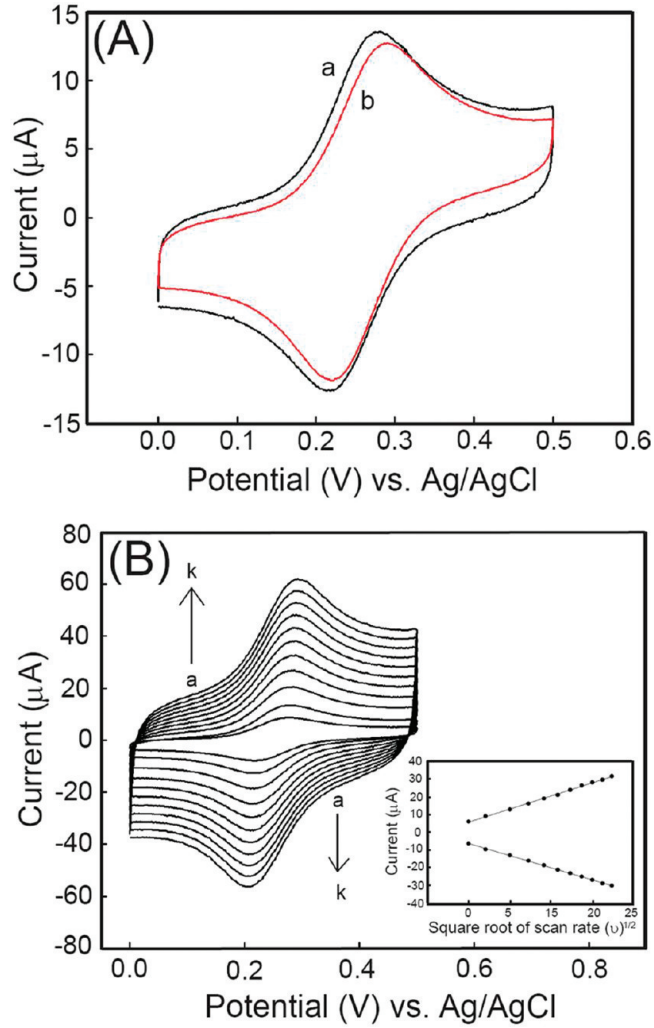

Figure 3. (A) CVs of (a) RGON and (b) OPH-RGON films in a solution of 5 mM $K_3Fe(CN)_6$ in 0.1 M KCl at a 50 mV/s scan rate and (B) CVs of RGON film in a solution of 5 mM $K_3Fe(CN)_6$ in 0.1 M KCl with different scan rates (a–k: 25, 50, 100, 150, 200, 250, 300, 350, 400, 450, and 500 mV/s). Inset is linear relationship of I_p and square root of scan rate (ν) at RGON film.

where i_p is the peak current, n is the number of charges, A is the area of the interface, D_o is the diffusion coefficient of the transferred species, C_o is the concentration, and υ is the scan rate.

It is worth noting that the linear relationship of i_p *versus* $\upsilon^{1/2}$ in RGON films is derived from the Nernstian behavior. A near-perfect scaling of the steady-state current in the diffusion controlled system was observed for the curves of the oxidation and reduction peak currents as a function of the square root of scan rates in the range of 25–500 mV in Figure 3B (R^2 is 0.9986 for I_{pa} and 0.9992 for I_{pc}, respectively). Consequently, a single electron Nernstian behavior in RGON films was attributed to semi-infinite linear diffusion at the surface of the electrode.[36,38]

To assess the applicability of a new electrochemical biosensor platform for the detection of paraoxon nerve agents, the electrochemical properties of RGON films were compared to those of pristine RGO. Paraoxon is

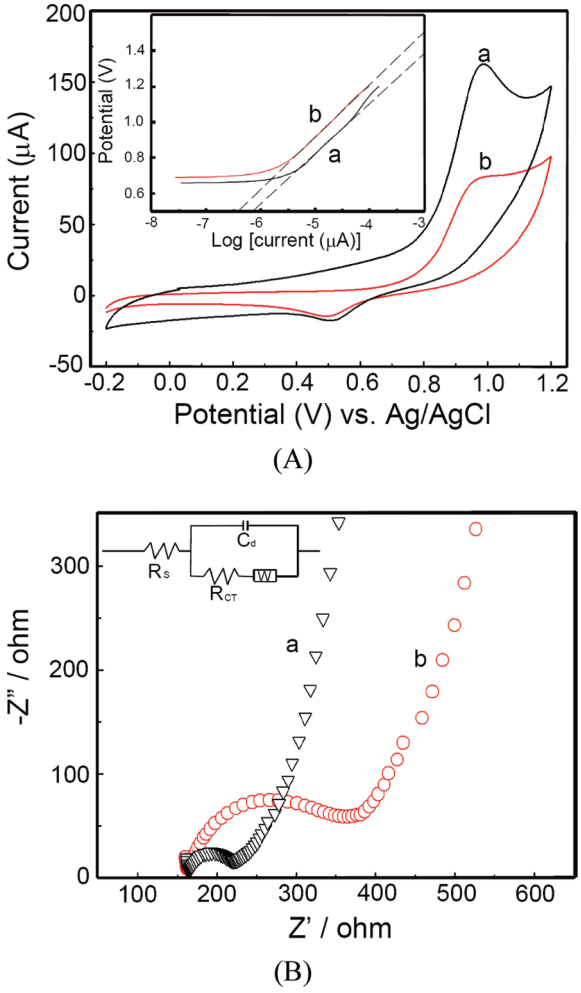

Figure 4. (A) CVs of (a) OPH-RGON and (b) OPH-RGO film in a solution of 1 mM paraoxon at a 50 mV/s scan rate (inset is the Tafel plots obtained from the CVs) and (B) Nyquist plot of (a) OPH-RGON and (b) OPH-RGO film (inset is the equivalent circuit with a Warburg impedance).

one of the most potent insecticides and chemical warfare agents, and thus monitoring this substance is important for protecting human health and warning potential terrorist attack.[40−42] ΔE_p of RGON films was slightly increased to 68 mV after the immobilization of OPH due to the resistance effect induced by biomolecule adsorption (Figure 3A). However, RGON films still showed a fast electron transfer reaction. Figure 4A displays CVs of RGO and RGON films for the detection of 1 mM paraoxon as a target molecule. Because of the facilitated electron transfer at the interface between RGON and the electrolyte, the oxidation peaks of paraoxon in hybrid films were significantly higher compared to those of RGO-coated films. The enhancement of charge transfer in RGONs can be explained by Tafel plots obtained from the reduced form of the Butler−Volmer eq 2,[37]

$$\log i = \log i_o + \frac{\alpha_A nF}{2.303RT}\eta \qquad (2)$$

where η is the overpotential, i is the exchange current density, α_A is the symmetry factor, and other symbols have conventional meanings. The shift in the onset potential for hybrid films was attributed to electronic equilibrium between two components. RGON and RGO films had slopes 277.3 and 290.2 mV/dec, respectively, in the region of the paraoxon reaction. Since the slope of the Tafel plot is related to the activation energy for the specific electrochemical reaction, facilitated charge transfer was confirmed by the observation of lower activation energy for RGON compared to RGO. To decouple the contributions of the bulk and interface to the overall resistance measurements, an equivalent circuit of hybrid films was analyzed by AC impedance as shown in Figure 4B. The charge transport resistance (R_{CT}) between the electrolyte and electrode is described by eq 3,[39]

$$Z(\omega) = R_s + \frac{R_{CT} + \sigma\omega^{-1/2}}{(C_d\sigma\omega^{1/2} + 1)^2 + \omega^2 C_d{}^2(R_{CT} + \sigma\omega^{-1/2})^2} - j\frac{\omega C_d(R_{CT} + \sigma\omega^{-1/2})^2 + \sigma\omega^{-1/2}(\sigma\omega^{1/2}C_d + 1)}{(C_d\sigma\omega^{1/2} + 1)^2 + \omega^2 C_d{}^2(R_{CT} + \sigma\omega^{-1/2})^2} \qquad (3)$$

where R_s is the solution resistance, C_d is the double layer capacitance, ω is the $2\pi f$, where f is the frequency, and σ is defined by

$$\sigma = \frac{RT}{\sqrt{2}F^2A}\left(\frac{1}{\sqrt{D_o C_o^*}} + \frac{1}{\sqrt{D_R C_R^*}}\right)$$

where A is the area of the electrode, D_o and D_R are the diffusion coefficients of oxidant and reductant, respectively, $C_o^*$and C_R^* are the bulk concentrations of oxidant and reductant, respectively, and other symbols have the usual meanings. R_{CT} of RGON (53 Ω) in the Nyquist plot was lower than that of RGO (181 Ω), indicating good electrical contact between the RGON film and electrolyte due to facilitated interfacial electron transfer.[37]

The superior qualities of self-assembled RGON films for electrochemical systems can be explained by the following lines of reasoning. Self-assembly of RGO by Nafion on the microscale generates a self-regulating interconnected architecture of hybrid films on a macroscopic scale. The interconnected network of RGOs exposed large basal planes toward the electrolyte solution at the interface, isolated by Nafion, while the wrinkled edges of RGO sheets coated by Nafion were curled or protruded from the surface. McCreery *et al.* reported that, in the two phase systems of the electrolyte and electrode, the ET kinetics was strongly influenced by the electronic structure of electrode.[43] In particular, the ideally crystalline basal planes of graphene had a low density of electronic states (DOS) at the Fermi level due to the small overlap of the valence and conduction bands, while the edge planes of graphene with many defect

TABLE 1. Sensitivities, Response Times, And Limit of Detections (LODs) of RGO, RGON, and f-RGON Biosensors

	sensitivity[a] (nA/μM)	response time[b] (s)	limit of detection[c] ($\times 10^{-7}$ M)
RGO	4.1	~10	13.9
RGON	10.7	~3	1.37
f-RGON[d]	9.7	~3	3.60

[a]Sensitivity was obtained from the calibration plots of the concentration of paraoxon and current signal. [b]Response time was determined when currents reach 95% of the steady-state state at each loading of paraoxon. [c]LOD was calculated from the characteristic signal-to-noise ratio ($S/N = 3$). [d]Fatigue test of RGON was performed by 100 bending cycles.

sites showed a high DOS at the Fermi level, resulting from the distribution of energies between the conduction and valence bands. Consequently, the edge planes of RGOs with a high DOS were directly responsible for the enhanced ET rates, while the large basal planes of Nafion-assembled RGOs led to the fast ET kinetics along three main lines of reason. First, the DOS of the basal planes of the self-assembled RGOs by Nafion could shift the Fermi level to a high DOS through electronic equilibrium at the interface. Considering that ET rates at the interface of the electrode and electrolyte are fastest when the Fermi levels of the two phases are equal,[43] a high DOS in the hybrid films can trigger a fast ET rate for the redox reaction. Second, the semimetallic character of the basal planes enhanced the ET rates due to high electron mobility at the interface where the edge planes directly contact the electrolyte solution. Third, the role of Nafion as an electrochemical binder between electrode and electrolyte created the good electrical contact or ideal wettability between the two phases being responsible for the fast ET kinetics. Therefore, the self-assembled RGON films serve as advanced conducting films due to a large accessible area, fast charge transfer, and low interfacial resistance for electrochemical reactions, as confirmed by TEM, SEM, CV, and impedance analysis.

Application into High Performance Electrochemical Biosensors. The performance characteristics of RGON-based electrochemical biosensors are determined by examining the amperometric response at a potential of +0.85 V during detection of the *p*-nitrophenol hydrolysis product of paraoxon. Figure 5A shows a comparison between the amperometric responses of OPH-RGON and OPH-RGO films to each successive addition of 2 μM paraoxon. In addition, the reliability of RGON biosensors was confirmed after 100 bending cycles in a fatigue test of RGON (f-RGON) as shown in Figure 5A and B. The biosensor sensitivity was obtained from the calibration plots of the concentration of paraoxon and current signal, which showed a perfect scaling of the steady-state current signals (R^2 is 0.9988). Table 1 summarizes the sensitivities, the response times, and the limit of detections (LODs) of RGO, RGON, and f-RGON biosensors. OPH-RGON films showed ~2.6-fold higher

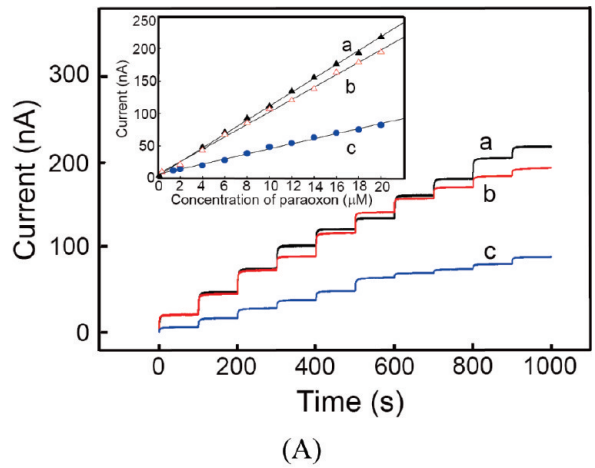

(A)

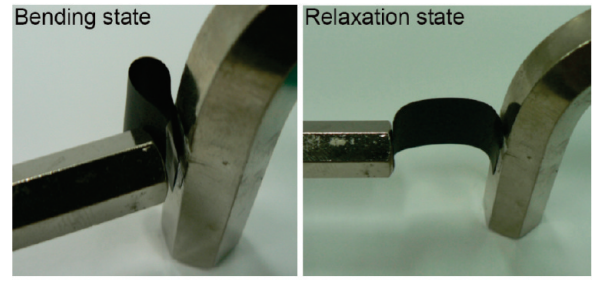

(B)

Figure 5. (A) Amperometric responses with respect to 2 μM increments of paraoxon in N_2-saturated PBS. Applied potential, +0.85 V: (a) OPH-RGON, (b) OPH-f-RGON, and (c) OPH-RGO films. The inset shows the calibration curves of the current signals with respect to the concentration of paraoxon. (B) Photo images of a fatigue test of RGON film.

sensitivity, 10.7 compared to 4.1 nA/μM for OPH-RGO. In addition, OPH-RGON biosensors reached 95% of the steady-state current within 3 s at each loading of paraoxon. The fast response time of RGON films was strongly related to the enhanced interfacial charge transfer in the diffusion-controlled system. The LOD of RGON biosensors (1.37×10^{-7} M) was 1 order of magnitude lower than that of RGO (1.39×10^{-6} M), as estimated from the characteristic signal-to-noise ratio ($S/N = 3$). Importantly, even after 100 bending cycles in f-RGON films, f-RGON films revealed a sensitivity of 9.7 nA/μM, LOD of 3.60×10^{-7} M, and response time of ~3 s, which were comparable to the maximum performance of RGON films (~90%) before the fatigue tests. RGO films could not perform bending tests because of their rupture or cracking from brittleness. These findings elucidate that the free-standing flexible conductive RGON films showed good sensing performance and reliability due to accelerated charge transfer and well-developed micro- and macroscale structures. The sensor performances of RGON biosensors were compared to the other types of sensors (see Supporting Information, Table S1). The RGON biosensors showed a higher sensitivity and faster response time than those of the unmodified electrodes such as thick film and gold elec-

trode, while the LOD values were similar.[40,41] The sensitivity of RGON biosensors was lower compared to that of the CNT-modified electrode,[42] presumably due to the intrinsic geometric differences between the one-dimensional and two-dimensional structures.[44,45] Nevertheless, RGON biosensors maintained ~90% of maximum sensor performance after 100 cycles of bending test. These results indicate that RGON films can be used as an advanced platform of high performance flexible biosensors including high sensitivity, fast response time, and low LOD.

CONCLUSION

We have demonstrated a facile and useful chemical approach for large-area free-standing flexible conductive hybrid films through a flow-directed assembly of RGON, which was prepared by the self-assembly of RGO with Nafion. Functionalization by Nafion *via* hydrophobic interactions provided a highly stable dispersibility of RGOs and mechanical integrity of the hybrid materials due to the intrinsic molecular structures and functionality of Nafion. From the perspective of electrochemical applications, RGON films exhibited Nernstian behavior, fast ET reaction, and low interfacial resistance. The excellent electrochemical and mechanical properties of RGON films make them suitable for biosensor platform applications, showing superior qualities, with a sensitivity of 10.7 nA/μM, detection limit of 1.37×10^{-7} M, and response time of <3 s for the detection of OP compounds. In particular, RGON films performed at ~90% of their maximum performance after fatigue tests of 100 bending cycles. The utility and versatility of concepts discussed here can be adapted to the development of graphene-based nanomaterials for emerging applications in flexible electronics.

EXPERIMENTAL SECTION

Chemicals. Graphite powder (<20 μM), hydrazine solution (35 wt % in water), and Nafion (perfluorinated resin solution, 5 wt % in lower aliphatic alcohol and water mixture) were purchased from Aldrich. 1-Propanol was obtained from Junsei.

Synthesis of Graphite Oxide (GO). GO was prepared from the graphite powder by the Hummers method. Prior to the preparation of GO, graphite powder (2 g) was mixed with a solution of H_2SO_4 (10 mL), $K_2S_2O_8$ (2 g), and P_2O_5 (2 g) at 85 °C, and the mixture was stirred for 5 h in order to obtain the preoxidized graphite. The mixtures were cooled to room temperature, added to deionized (DI) water (500 mL), and left overnight. The mixtures were washed with DI water under vacuum filtration and dried under vacuum at room temperature. The as-prepared products were put into a stirred cold solution of H_2SO_4 (100 mL) while cooling in an ice−water bath. This resulting slurry was gradually added to $KMnO_4$ (10 g) in a stirred system with an ice−water bath for 1 h. The mixtures were then stirred at room temperature for 24 h, followed by mixing with the DI water (500 mL) and 30% H_2O_2 (20 mL). The color of the mixtures changed to brilliant yellow with bubbling. After resulting mixture was filtrated, the precipitate was subsequently washed with 10 wt % of aqueous HCl solution (1 L) to remove remaining metal ions, followed by washing with DI water (1 L) to remove the acid. The as-obtained graphite oxide powders were diluted with DI water and purified thoroughly by dialysis for 1 week to remove remaining impurities until the filtrated solution was neutral. The powder was then filtered, washed with DI water several times, and dried at 60 °C under vacuum. Prior to the preparation of RGON, dry GOs (10 mg) were fully exfoliated in DI water (10 mL) by ultrasonic treatment for 30 min (Fisher Scientific model 500 ultrasonic, 350 W). The complete exfoliation of GOs was confirmed by TEM and AFM analyses as shown in Supporting Information, Figure S4.

Fabrication of RGON Films. To fabricate RGON hybrids, the exfoliated GOs were dispersed in the solution of DI water and 1-propanol (volume ratio of 50:50). Varying weight ratios of Nafion (0.1−50 wt %) were mixed with 0.5 mg/mL of GOs in 20 mL of DI water/1-propanol bisolvents (volume ratio of 50:50). The homogeneous solution of GO and Nafion was prepared by sonication for 60 min. A highly homogeneous black dispersion was obtained after reduction was achieved by the addition of 100 μL of hydrazine solution at 85 °C for 24 h. The resulting mixture was washed with DI water and ethanol several times, and the RGON hybrids were purified by dialysis for 1 week to remove the remaining hydrazine and impurities. Finally, the powder was filtered and dried under vacuum at room temperature and stored.

RGON films were prepared by filtering homogeneous solutions in DI water/1-propanol (volume ratio of 50:50) bisolvents through an anodizc membrane filter (47 mm in diameter, 0.2 μm pore size, Whatman). The resulting films were dried in air and peeled off of the filter membrane, reported in the method for preparation of GO papers. For investigating electrochemical performance, the RGON films were transferred to a glass substrate. A 10 μL portion of organophosphorus hydrolase (OPH), 1 mg/mL, was dropped on the surface of the RGON film, dried under room temperature for 12 h, and washed with phosphate-buffered saline (PBS, pH 7.4) to remove excess enzyme molecules. The as-prepared OPH-immobilized RGON films (OPH-RGONs) were dried at room temperature under vacuum for use as biosensor platforms. OPH-RGOs as control samples were prepared following the same protocols as OPH-RGONs.

Production of Mature OPH in *Escherichia coli*. Polymerase chain reactions (PCRs) were performed using a PCR Thermal Cycler (Bio-Rad, Hercules, CA) and a High Fidelity PCR System (Boehringer Mannheim, Mannheim, Germany). Restriction and DNA modifying enzymes were purchased from New England Biolabs (Berverly, MA). The DNA sequences of all clones were confirmed by automatic DNA sequencer (ABI Prism model 377, Perkin-Elmer Co., IL). An OPH was used as a model protein for convenient immobilization onto the RGO and RGON films and for the hydrolysis of paraoxon. Six histidine (6His) residues were introduced for easy purification of mature OPH (mOPH), which was accomplished by immobilized metal affinity chromatography. For the cloning and expression of the mOPH gene (NCBI accession no. AY766084), a PCR amplification experiment was carried out using the primers P1 (5′-GAAATTCCATATG*CATCATCACCACCA-CCAC*GGATCGATCGGCACAGGCGA-3′) and P2 (5′-AAAACTCGAGTGACGCCCGCAAGGTCGGTGA-3′) (underlines indicate the restriction enzyme sites and italics denote the coding sequence for six histidines), and the genomic DNA of *Flavobacterium* sp. ATCC 27551 as a template. After the PCR product of the mOPH gene was digested with *Nde*I and *Xho*I, it was ligated into the sites of pET-22b(+) (Novagen, San Diego, CA) to make pET-mOPH. For the production of mOPH, *E. coli* BL21(DE3) (F^- *ompT hsdS*$_B$ (r_B^- m_B^-) *gal dcm* (DE3), Novegen harboring pET-mOPH was cultivated in 100 mL of Luria−Bertani (LB) medium (10 g/L tryptone, 5 g/L yeast extract, 5 g/L NaCl), which was supplemented with ampicillin (Ap, 100 μg/mL) in a shaking incubator at 37 °C and 200 rpm. After the addition of isopropyl-β-D-thiogalactopyranoside (IPTG, Sigma), cells were further cultivated for 6 h. Cells were harvested and disrupted by sonication (Braun Ultrasonics Co, Danbury, CT) for 1 min at 20% output. After the centrifugation of cell suspension at 16000*g* for 10 min at 4 °C, the pellet containing the insoluble protein fraction was

saved for the purification of the proteins. Ni-NTA column (Qiagen, Valencia, CA) was used for the purification of mOPH proteins without further purification steps. The concentration of protein was determined by Bradford's method using bovine serum albumin (BSA, Sigma) as a standard.

Characterization. Transmission electron microscope (TEM) images were collected on an E.M. 912 Ω energy-filtering TEM (EF TEM 120 kV) and a JEM-3010 HR TEM (300 kV). The scanning electron microscope (SEM) micrographs were obtained using a field emission scanning electron microscope (FEI Sirion model) equipped with an in-house Schottky emitter in high stability. The atomic force microscopy (AFM) images were recorded in the noncontact mode using a Nanoman Digital Instruments 3100 AFM (VEECO) with an etched silicon aluminum coated tip. The Fourier transform infrared (FT-IR) attenuated total reflection (ATR) spectra were collected on a JASCO FT-IR 470 plus as attenuated total reflection. Each spectrum was recorded from 4000 to 650 cm^{-1} using 12 scans at a resolution of 4 cm^{-1}. The pressure was equal in all samples to avoid differences caused by the pressure and penetrating depth. The X-ray diffraction (XRD) data were obtained on a Rigaku D/max IIIC (3 kW) with a θ/θ goniometer equipped with a Cu Kα radiation generator. The diffraction angle of the diffractograms was in the range of $2\theta = 5°-40°$. Solid-state magic angle spinning (MAS) nuclear magnetic resonance (NMR) spectra were collected on a Bruker Avance 400 spectrometer operating at 10 kHz using a 4 mm MAS. Spectra based on free induction decays with moderate decoupling power were averaged over 4000 scans with a recycle delay of 4 s. The Raman spectra were recorded from 3500 to 100 cm^{-1} on a Bruker FT Raman spectrophotometer RFS 100/S using a 785 and 1064 nm dual channel laser at a resolution of 1 cm^{-1}. The X-ray photoelectron spectroscopy (XPS) data were obtained using a Thermo MultiLab 2000 system. Al Mgα X-ray source at 200 W was used with pass energy of 20 eV and 45° takeoff angle under 10^{-7} Torr vacuum analysis chamber. The high resolution scans of C and low resolution survey scans were analyzed for each sample at least at two separated locations. The zeta potentials of RGO and RGON solutions were measured by a Malvern Zetasizer Nano-ZS particle analyzer. CV and AC impedance were analyzed by a CHI660C electrochemical workstation (CH Instruments) with a conventional three-electrode electrochemical cell using an RGO- and RGON-contacted working electrode, a KCl−Ag/AgCl reference electrode, and a platinum wire counter-electrode. All potentials reported here are given with respect to the reference electrode. AC impedance was carried out in the range from 0.1 Hz to 100 kHz at constant 10 mV amplitude. The amperometric responses were performed in N_2-saturated PBS at a constant potential of 0.85 V from the hydrodynamic voltammetric data. Electrical conductivities of RGO and RGON films were measured by using the standard 4-point probe technique (Loresta-GP, Mitsubishi Chemical). All electrochemical data were obtained at room temperature within the error range of ±5%. Mechanical property tests were performed by a dynamic mechanical analyzer (DMA Q800, TA Instruments) at room temperature. The samples were cut with a razor blade into rectangular strips of approximately 3×15 mm^2 for mechanical testing and were gripped using film tension clamps with a clamp compliance of 0.2 μm/N. All tensile tests were conducted in controlled strain rate mode with a preload of 0.01 N and a strain ramp rate of 0.05%/min. Tensile modulus was determined by fitting the stress−strain plot in the elastic regime with a straight line.

Acknowledgment. This work was supported in part by the IT Leading R&D Support Project from the MKE through KEIT, and by the KOSEF through the Center for Ultramicrochemical Process Systems. We thank the National NanoFab Center (NNFC) for the use of equipment for TEM, SEM, and AFM measurements.

Supporting Information Available: Supporting figures and spectra; table listing performance of various sensors. This material is available free of charge *via* the Internet at http://pubs.acs.org.

REFERENCES AND NOTES

1. Novoselov, K. S.; Geim, A. K.; Morozov, S. V.; Jiang, D.; Zhang, Y.; Dubonos, S. V.; Grigorieva, I. V.; Firsov, A. A. Electric Field Effect in Atomically Thin Carbon Films. *Science* **2004**, *306*, 666–669.
2. Li, X.; Wang, X.; Zhang, L.; Lee, S.; Dai, H. Chemically Derived, Ultrasmooth Graphene Nanoribbon Semiconductors. *Science* **2008**, *319*, 1229–1232.
3. Lu, J.; Drzal, L. T.; Worden, R. M.; Lee, I. Simple Fabrication of a Highly Sensitive Glucose Biosensor Using Enzymes Immobilized in Exfoliated Graphite Nanoplatelets Nafion Membrane. *Chem. Mater.* **2007**, *19*, 6240–6246.
4. Wang, X.; Zhi, L.; Müllen, K. Transparent, Conductive Graphene Electrodes for Dye-Sensitized Solar Cells. *Nano Lett.* **2008**, *8*, 323–327.
5. Schedin, F.; Geim, A. K.; Morozov, S. V.; Hill, E. W.; Blake, P.; Katsnelson, M. I.; Novoselov, K. S. Detection of Individual Gas Molecules Adsorbed on Graphene. *Nat. Mater.* **2007**, *6*, 652–655.
6. Bunch, J. S.; Zande, A. M.; Verbridge, S. S.; Frank, I. W.; Tanenbaum, D. M.; Parpia, J. M.; Craighead, H. G.; McEuen, P. L. Electromechanical Resonators from Graphene Sheets. *Science* **2007**, *315*, 490–493.
7. Ramanathan, T.; Abdala, A. A.; Stankovich, S.; Dikin, D. A.; Herrera-Alonso, M.; Piner, R. D.; Adamson, D. H.; Schniepp, H. C.; Chen, X.; Ruoff, R. S.; *et al*. Functionalized Graphene Sheets for Polymer Nanocomposites. *Nat. Nanotechnol.* **2008**, *3*, 327–331.
8. Yoo, E.; Kim, J.; Hosono, E.; Zhou, H.-S.; Kudo, T.; Honma, I. Large Reversible Li Storage of Graphene Nanosheet Families for Use in Rechargeable Lithium Ion Batteries. *Nano Lett.* **2008**, *8*, 2277–2282.
9. Stoller, M. D.; Park, S.; Zhu, Y.; An, J.; Ruoff, R. S. Graphene-Based Ultracapacitors. *Nano Lett.* **2008**, *8*, 3498–3502.
10. Chen, W.; Chen, S.; Qi, D. C.; Gao, X. Y.; Wee, A. T. S. Surface Transfer p-Type Doping of Epitaxial Graphene. *J. Am. Chem. Soc.* **2007**, *129*, 10418–10422.
11. Li, D.; Müller, M. B.; Gilje, S.; Kaner, R. B.; Wallace, G. G. Processable Aqueous Dispersions of Graphene Nanosheets. *Nat. Nanotechnol.* **2008**, *3*, 101–105.
12. Park, S.; Ruoff, R. S. Chemical Methods for the Production of Graphenes. *Nat. Nanotechnol.* **2009**, *4*, 217–224.
13. Park, S.; An, J.; Piner, R. D.; Jung, I.; Yang, D.; Velamakanni, A.; Nguyen, S. T.; Ruoff, R. S. Aqueous Suspension and Characterization of Chemically Modified Graphene Sheets. *Chem. Mater.* **2008**, *20*, 6592–6594.
14. Shen, J.; Hu, Y.; Li, C.; Qin, C.; Ye, M. Synthesis of Amphiphilic Graphene Nanopatelets. *Small* **2009**, *5*, 82–85.
15. Si, Y.; Samulski, E. T. Synthesis of Water Soluble Graphene. *Nano Lett.* **2008**, *8*, 1679–1682.
16. Xu, Y.; Bai, H.; Lu, G.; Li, C.; Shi, G. Flexible Graphene Films *via* the Filtration of Water-Soluble Noncovalent Functionalized Graphene Sheets. *J. Am. Chem. Soc.* **2008**, *130*, 5856–5857.
17. Lomeda, J. R.; Doyle, C. D.; Kosynkin, D. V.; Hwang, W.-F.; Tour, J. M. Diazonium Functionalization of Surfactant-Wrapped Chemically Converted Graphene Sheets. *J. Am. Chem. Soc.* **2008**, *130*, 16201–16206.
18. Xu, Y.; Liu, Z.; Zhang, X.; Wang, Y.; Tian, J.; Huang, Y.; Ma, Y.; Zhang, X.; Chen, Y. A. Graphene Hybrid Material Covalently Functionalized with Porphyrin: Synthesis and Optical Limiting Property. *Adv. Mater.* **2009**, *21*, 1275–1279.
19. Patil, A. J.; Vickery, J. L.; Scott, T. B.; Mann, S. Aqueous Stabilization and Self-Assembly of Graphene Sheets into Layered Bio-nanocomposites using DNA. *Adv. Mater.* **2009**, *21*, 3159–3164.
20. Landi, B. J.; Raffaelle, R. P.; Heben, M. J.; Alleman, J. L.; VanDerveer, W.; Gennett, T. Single Wall Carbon Nanotube−Nafion Composite Actuators. *Nano Lett.* **2002**, *2*, 1329–1332.
21. Shim, B. S.; Chen, W.; Doty, C.; Xu, C.; Kotov, N. A. Smart Electronic Yarns and Wearable Fabrics for Human

Biomonitoring made by Carbon Nanotube Coating with Polyelectrolytes. *Nano Lett.* **2008**, *8*, 4151–4157.
22. Wang, J.; Musameh, M.; Lin, Y. Solubilization of Carbon Nanotubes by Nafion toward the Preparation of Amperometric Biosensors. *J. Am. Chem. Soc.* **2003**, *125*, 2408–2409.
23. Lu, J.; Do., I.; Drzal, L. T.; Worden, R. M.; Lee, I. Nanometal-Decorated Exfoliated Graphite Nanoplatelet Based Glucose Biosensors with High Sensitivity and Fast Response. *ACS Nano* **2008**, *2*, 1825–1832.
24. Luo, C.; Zuo, X.; Wang, L.; Wang, E.; Song, S.; Wang, J.; Wang, J.; Fan, C.; Cao, Y. Flexible Carbon Nanotube−Polymer Composite Films with High Conductivity and Superhydrophobicity Made by Solution Process. *Nano Lett.* **2008**, *8*, 4454–4458.
25. Shan, C.; Yang, H.; Song, J.; Han, D.; Ivaska, A.; Niu, L. Direct Electrochemistry of Glucose Oxidase and Biosensing for Glucose Based on Graphene. *Anal. Chem.* **2009**, *81*, 2378–2382.
26. Mauritz, K. A.; Moore, R. B. State of Understanding of Nafion. *Chem. Rev.* **2004**, *104*, 4535–4586.
27. Hummers, W. S.; Offeman, R. E. Preparation of Graphitic Oxide. *J. Am. Chem. Soc.* **1958**, *80*, 1339.
28. Lee, J.-H; Paik, U; Choi, J.-Y; Kim, K. K.; Yoon, S.-M.; Lee, J.; Kim, B.-K.; Kim, J. M.; Park, M. H.; Yang, C. W.; *et al*. Dispersion Stability of Single-Walled Carbon Nanotubes Using Nafion in Bisolvent. *J. Phys. Chem. C* **2007**, *111*, 2477–2483.
29. Zhang, J.; Gao, L.; Sun, J.; Liu, Y.; Wang, Y.; Wang, J.; Kajiura, H.; Li, Y.; Noda, K. Dispersion of Single-Walled Carbon Nanotubes by Nafion in Water/Ethanol for Preparing Transparent Conducting Films. *J. Phys. Chem. C* **2008**, *112*, 16370–16376.
30. Wu, Z.; Chen, Z.; Du, X.; Logan, J. M.; Sippel, J.; Nikolou, M.; Kamaras, K.; Reynolds, J. R.; Tanner, D. B.; Hebard, A. F.; Rinzler, A. G. Transparent, Conductive Carbon Nanotube Films. *Science* **2004**, *305*, 1273–1276.
31. He, F.; Lau, S.; Chan, H. L.; Fan, J. High Dielectric Permittivity and Low Percolation Threshold in Nanocomposites Based on Poly(vinylidene fluoride) and Exfoliated Graphite Nanoplates. *Adv. Mater.* **2009**, *21*, 710–715.
32. Everett, D. H. *Basic Principles of Colloid Science*; The Royal Society of Chemistry: London, 1998.
33. Dikin, D. A.; Stankovich, S.; Zimney, E. J.; Piner, R. D.; Dommett, G. H. B.; Evmenenko, G.; Nguyen, S. T.; Ruoff, R. S. Preparation and Characterization of Graphene Oxide Paper. *Nature* **2007**, *448*, 457–460.
34. Maleki, N.; Safavi, A.; Tajabadi, F. High-Performance Carbon Composite Electrode Based on an Ionic Liquid as a Binder. *Anal. Chem.* **2006**, *78*, 3820–3826.
35. Kachoosangi, R. T.; Musameh, M. M.; Abu-Yousef, I.; Yousef, J. M.; Kanan, S. M.; Xiao, L.; Davies, S. G.; Russell, A.; Compton, R. G. Carbon Nanotube−Ionic Liquid Composite Sensors and Biosensors. *Anal. Chem.* **2009**, *81*, 435–442.
36. Nugent, J. M.; Santhanam, K. S. V.; Rubio, A.; Ajayan, P. M. Fast Electron Transfer Kinetics on Multiwalled Carbon Nanotube Microbundle Electrodes. *Nano Lett.* **2001**, *1*, 87–91.
37. Bard, A. J.; Faulkner, L. R. *Electrochemical Methods. Fundamentals and Applications*, 2nd ed.; John Wiley & Sons: New York, 2001.
38. Shang, N. G.; Papakonstantinou, P.; McMullan, M.; Chu, M.; Stamboulis, A.; Potenza, A.; Dhesi, S. S.; Marchetto, H. Catalyst-Free Efficient Growth, Orientation and Biosensing Properties of Multilayer Graphene Nanoflake Films with Sharp Edge Planes. *Adv. Funct. Mater.* **2008**, *18*, 3506–3514.
39. Chang, B.-Y.; Park, S.-M. Integrated Description of Electrode/Electrolyte Interfaces Based on Equivalent Circuits and Its Verification Using Impedance Measurements. *Anal. Chem.* **2006**, *78*, 1052–1060.
40. Mulchandani, A.; Mulchandani, P.; Chen, W.; Wang, J.; Chen, L. Amperometric Thick-Film Strip Electrodes for Monitoring Organophosphate Nerve Agents Based on Immobilized Organophosphorus Hydrolase. *Anal. Chem.* **1999**, *71*, 2246–2249.
41. Wang, J.; Krause, R.; Block, K.; Musameh, M.; Mulchandani, A.; Schöning, M. J. Flow Injection Amperometric Detection of OP Nerve Agents Based on an Organophosphorus-Hydrolase Biosensor Detector. *Biosens. Bioelectron.* **2003**, *18*, 255–260.
42. Deo, R. P.; Wang, J.; Block, I.; Mulchandani, A.; Joshi, K. A.; Trojanowicz, M.; Scholz, F.; Chen, W.; Lin, Y. Determination of Organophosphate Pesticides at a Carbon Nanotube/Organophosphorus Hydrolase Electrochemical Biosensor. *Anal. Chim. Acta* **2005**, *530*, 185–189.
43. McCreery, R. L. Advanced Carbon Electrode Materials for Molecular Electrochemistry. *Chem. Rev.* **2008**, *108*, 2646–2687.
44. Gruner, G. Carbon Nanotube Transistors for Biosensing Applications. *Anal. Bioanal. Chem.* **2006**, *384*, 322–335.
45. Allen, B. L.; Kichambare, P. D.; Star, A. Carbon Nanotube Field-Effect-Transistor-Based Biosensors. Adv. Mater. 2007, *19*, 1439−1451.